Supporting Information for

Size-dependent antiferromagnetism and direct observation of Néel axes in NiO nanoparticles

Jorge Ara,[a,b] *Carlos Moya,*[a-c*] *Montserrat García del Muro,*[a,b] *Adriana I. Figueroa,*[a,b] *Marta X. Aribó,*[a,b] *Òscar Iglesias,*[a,b] *Armin Kleibert,*[d] *Amílcar Labarta,*[a,b] *Arantxa Fraile Rodríguez,*[a,b*]*, and Xavier Batlle*[a,b]*

[a] Departament de Física de la Matèria Condensada, Universitat de Barcelona, Martí i Franquès 1, 08028 Barcelona, Spain

[b] Institut de Nanociència i Nanotecnologia (IN2UB), Universitat de Barcelona, 08028 Barcelona, Spain

[c] Departament de Química Inorgànica i Orgànica, Universitat de Barcelona, Martí i Franquès, 1-11, 08028 Barcelona, Spain

[d] Swiss Light Source, Paul Scherrer Institut, Villigen, PSI CH-5232, Switzerland

Corresponding authors: carlosmoyaalvarez@ub.edu, arantxa.fraile@ub.edu, xavierbatlle@ub.edu

Table of contents:

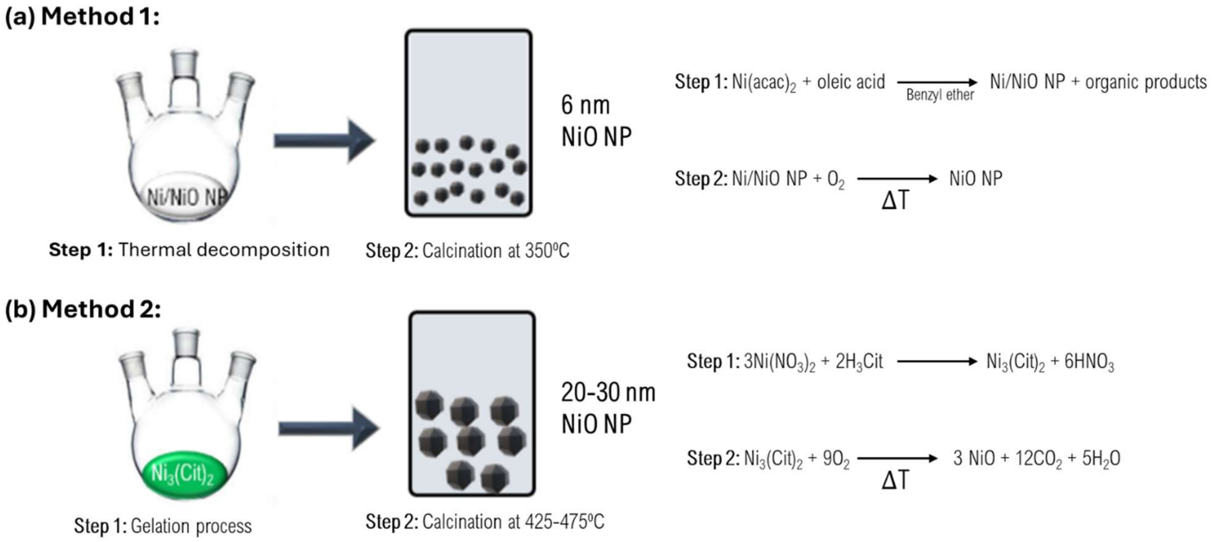

Figure S1. Comparative synthesis methods for NiO NP. (a) Method 1: A two-step synthesis process producing 6 nm NiO NP, initiated by thermal decomposition of $Ni(acac)_2$ to produce Ni/NiO NP, followed by calcination at 350°C. (b) Method 2: Gelation process to form $Ni_3(Cit)_2$ and its subsequent calcination in the range of 425-475°C to obtain 20-30 nm NiO NP.

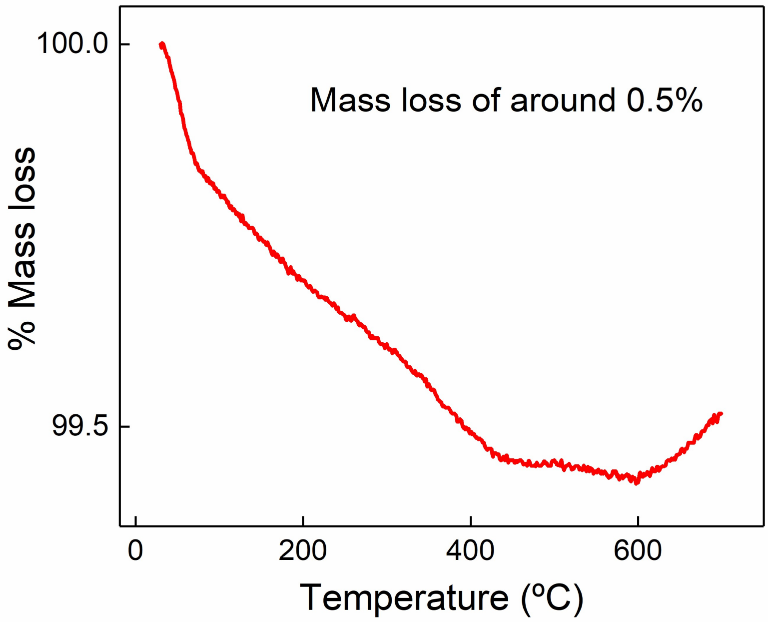

Figure S2. TG graph of the sample NiO30 from RT to 700 ºC with a heating rate of 10 ºC·min^{-1} under nitrogen atmosphere.

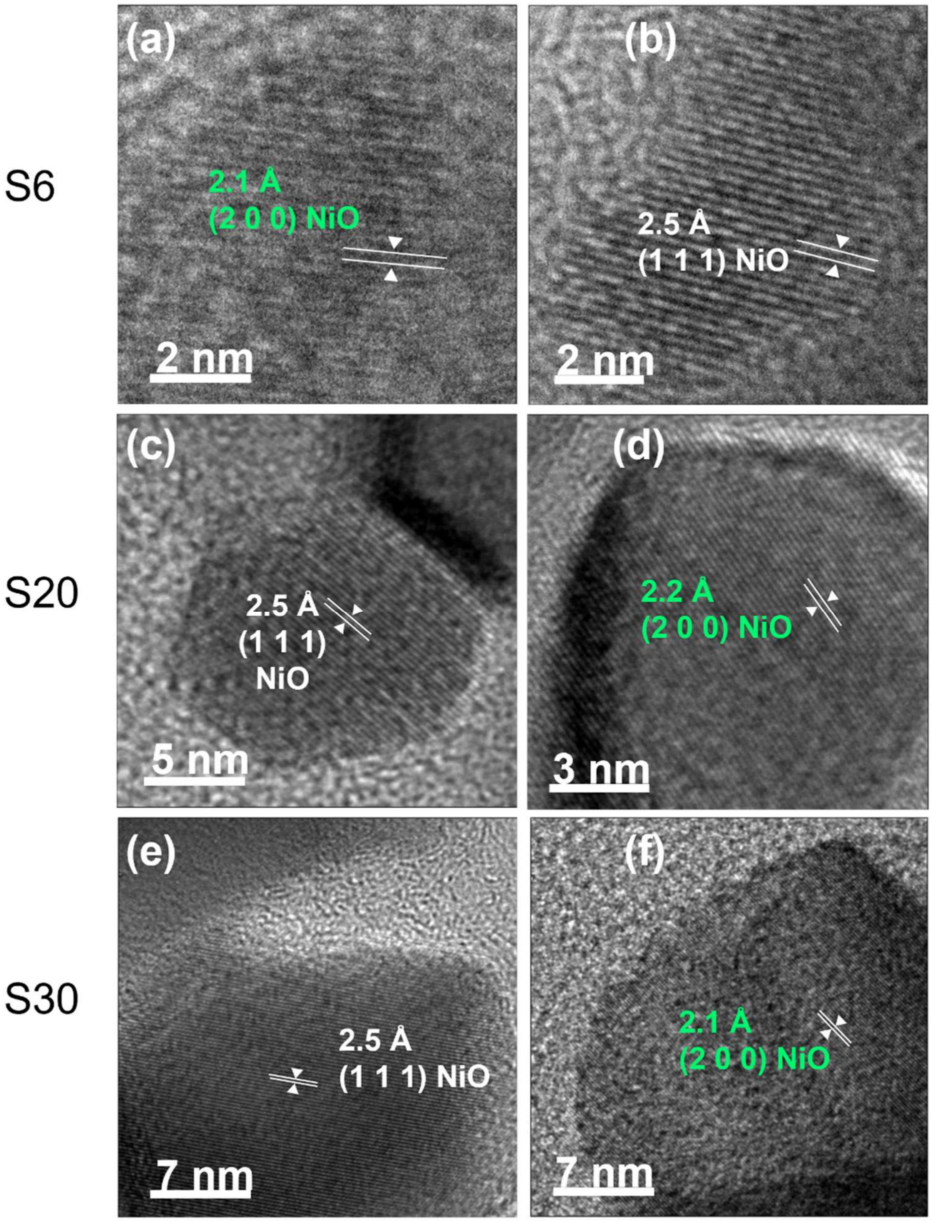

Figure S3. Gallery of HRTEM images.

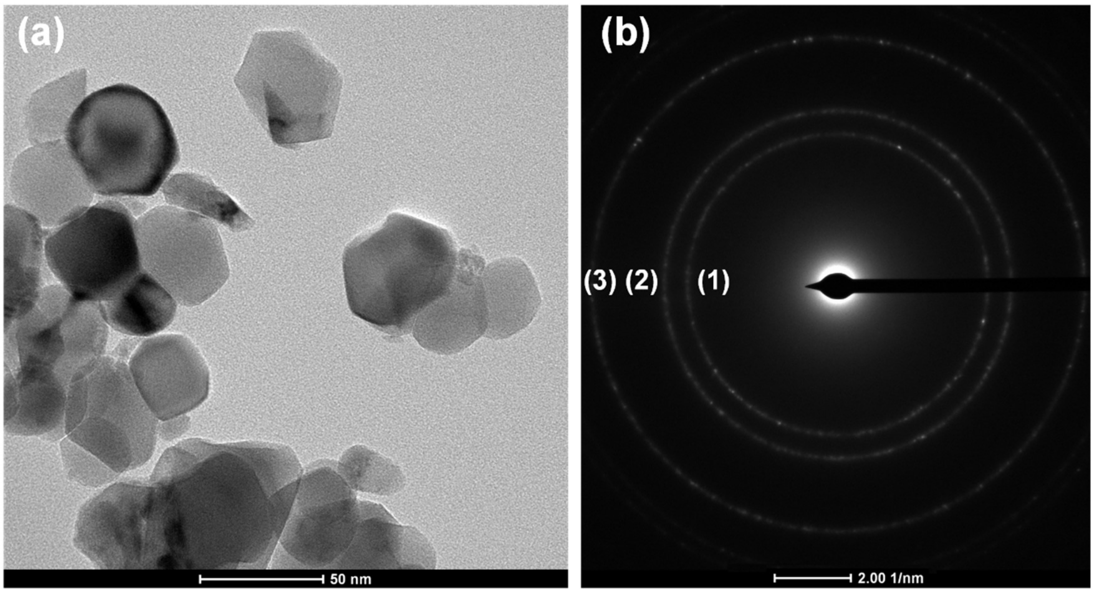

(c)

Rings	d-spacing (Å)	NiO reference (Å)	NiO plane	% var. NiO
1	2.59(1)	2.41	111	7.5
2	2.25(1)	2.08	200	8.2
3	1.58(1)	1.47	220	7.5

Figure S4. (a) Low-resolution TEM image of the sample NiO30 and its corresponding SAED pattern (b). Table (c) shows the estimated d-spacings together with the NiO reference values extracted from ICSD 01-071-1179.

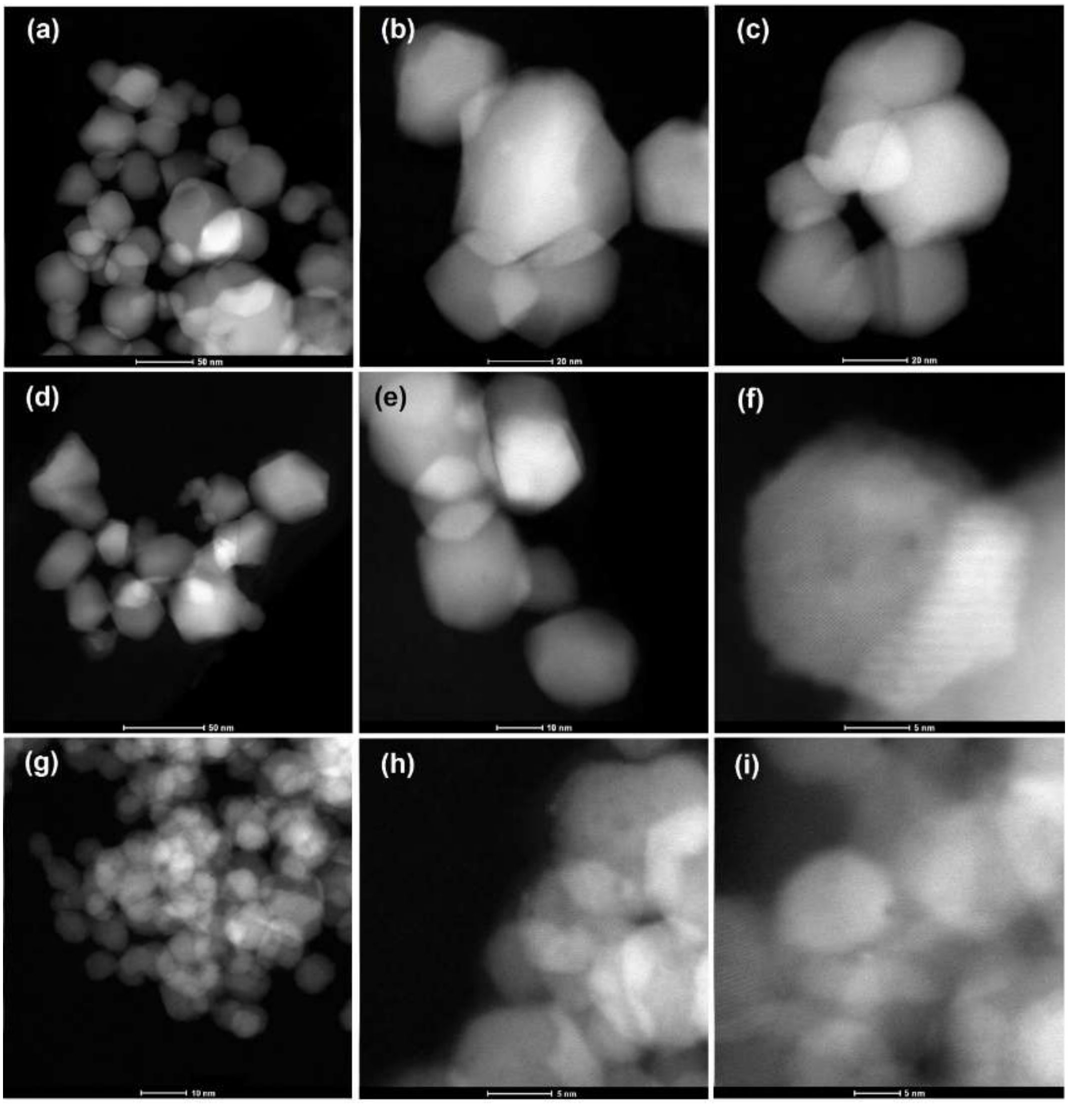

Figure S5. Gallery of HAADF images ranging from low resolution to HRTEM (from left-hand side to right-hand panels) of samples NiO30 (a-c), NiO20 (d-f), and NiO6 (g-i).

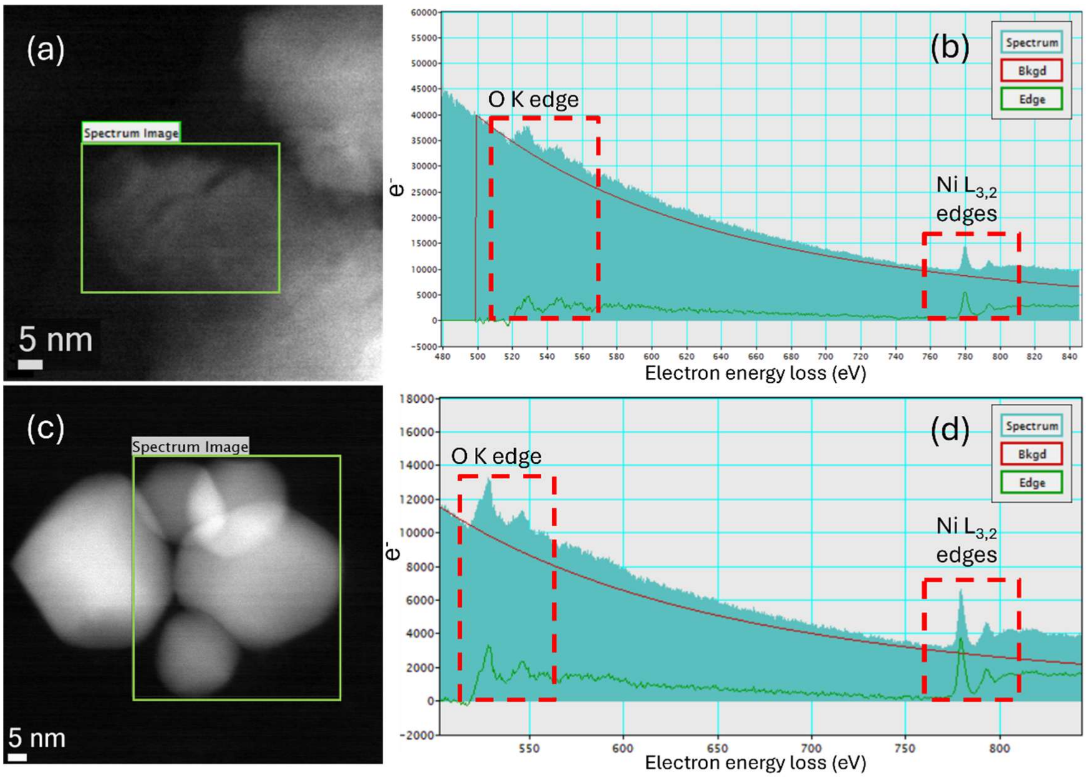

Figure S6. Compositional EELS analysis of the sample NiO30. (b) and (d) show the fitted EELS spectra of corresponding scanned areas consisting of single particle (a) and mildly agglomerated (c) areas. The obtained Ni:O atomic ratios for regions (a) and (c) are 0.8(1) and 1.0(1), respectively.

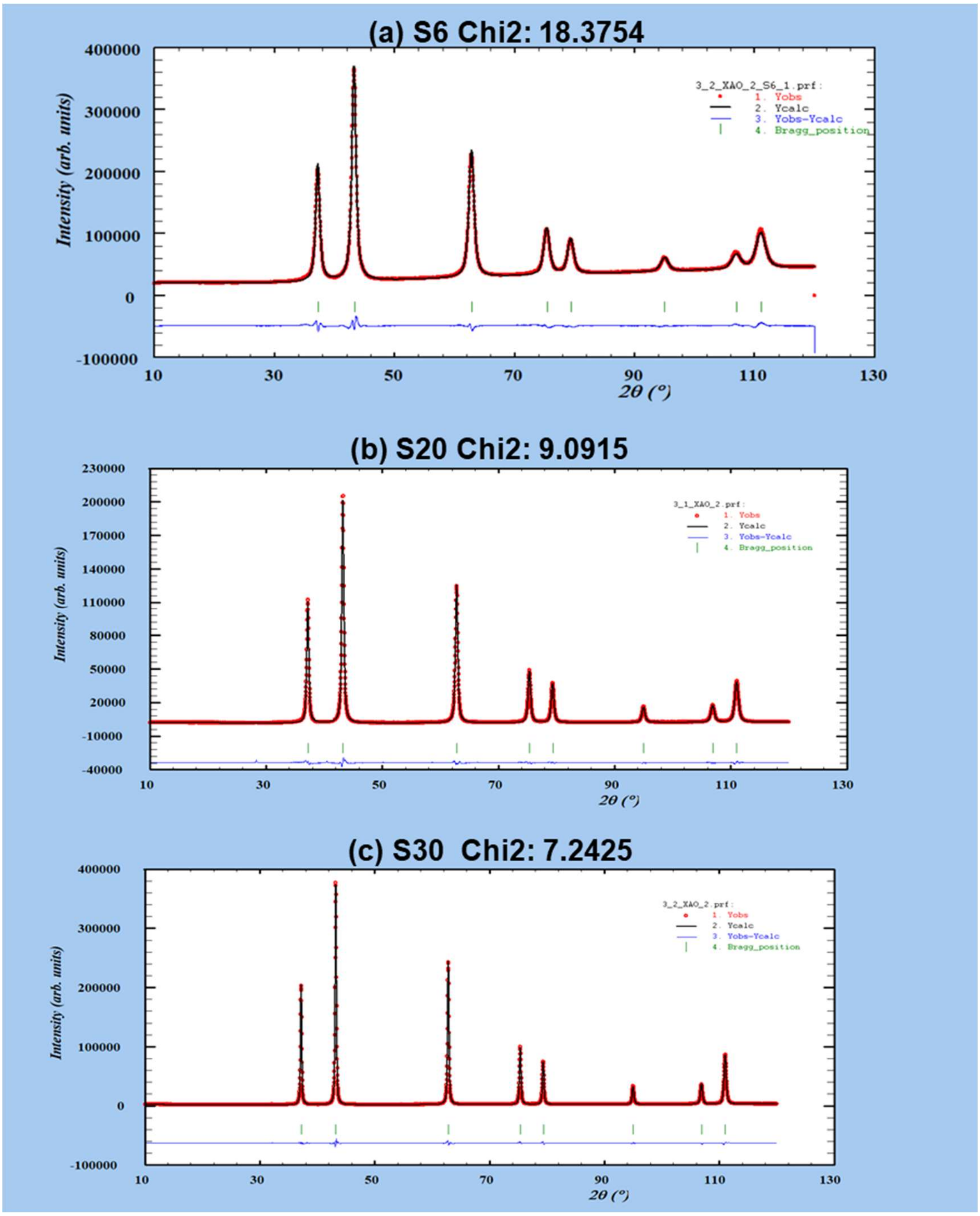

Figure S7. Rietveld refinements of the XDR patterns of samples NiO6 (a), NiO20 (b), and NiO30 (c), showing Chi2 values within 7 and 18, which indicates high quality fits.

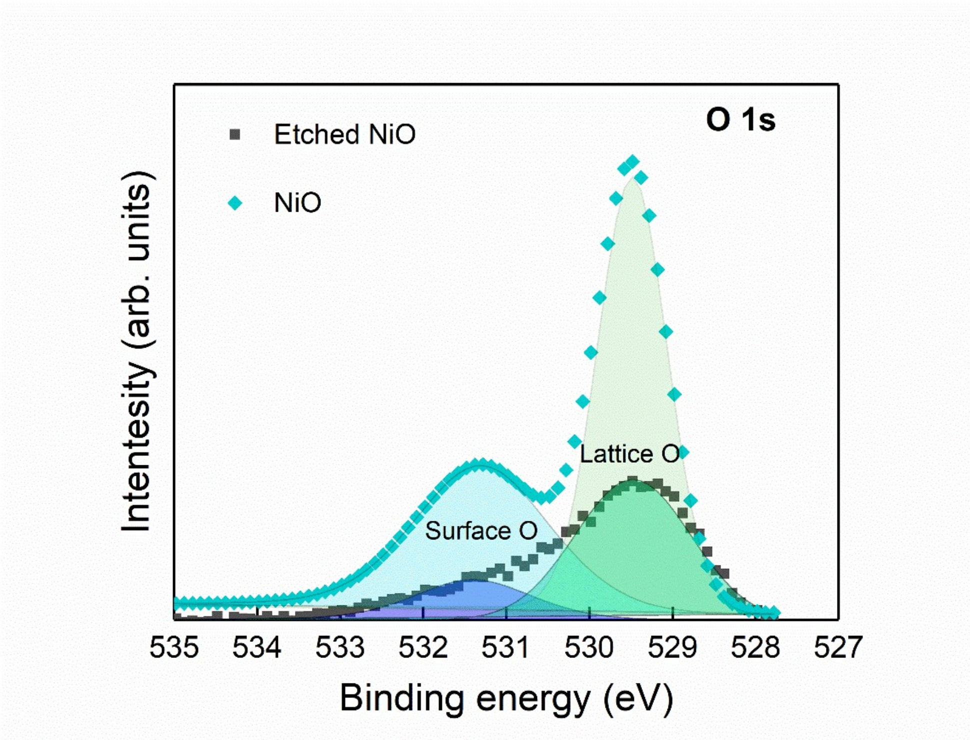

Figure S8. XPS spectra of sample NiO30 before etching (rhombus) and after 120 min of 0.5 kV Ar ion etching (squares). The decrease of the 'Surface O' signal respect to the 'Lattice O' can easily be appreciated.

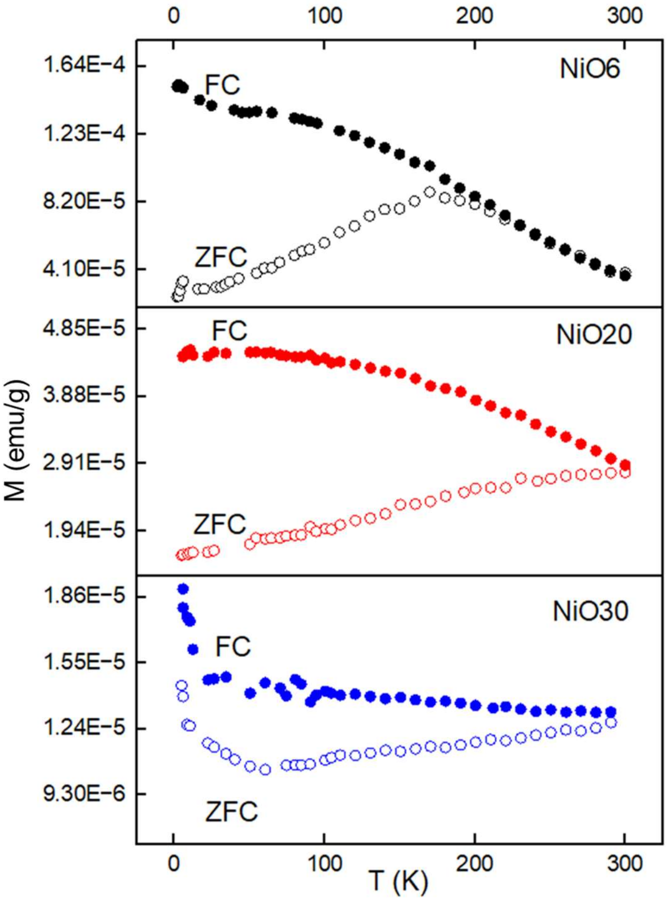

Figure S9. $M_{ZFC} - M_{FC}$ measurements of the magnetization as a function of temperature under a magnetic field of 50 Oe. The symbols are as follows: NiO6 (black), NiO20 (red), and NiO30 (blue). M_{ZFC} are shown in empty symbols, while M_{FC} are shown in solid spheres.

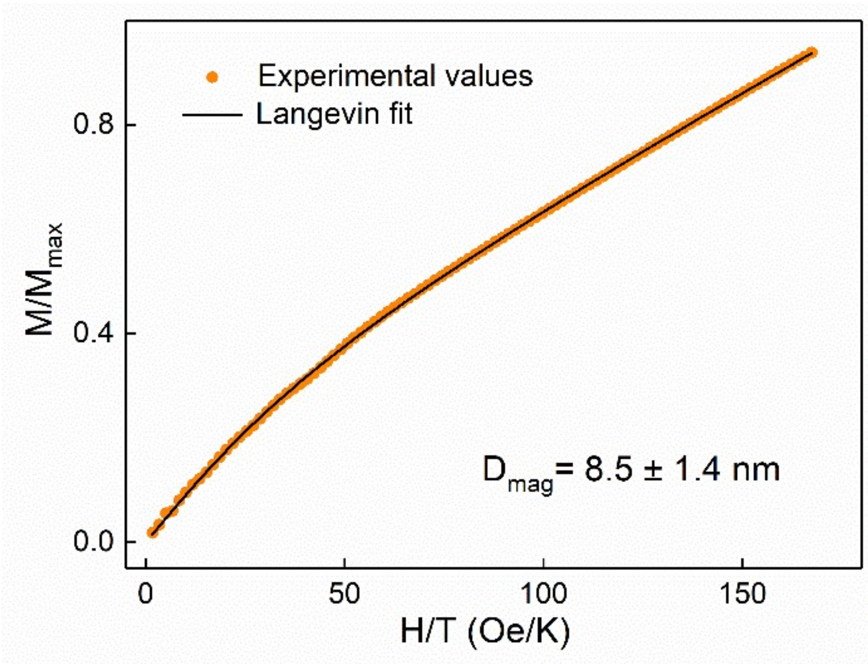

Figure S10. Normalized magnetization $\left({}^{M}/_{M_{max}}\right)$ versus reduced magnetic field $\left({}^{H}/_{T}\right)$ at room temperature for sample NiO6. The plot depicts experimental values (orange symbols) fitted by a distribution of Langevin functions (solid black line), showing the superparamagnetic behavior of the particles. Computed mean magnetic diameter D_{mag} is 8.5 ± 1.4 nm.

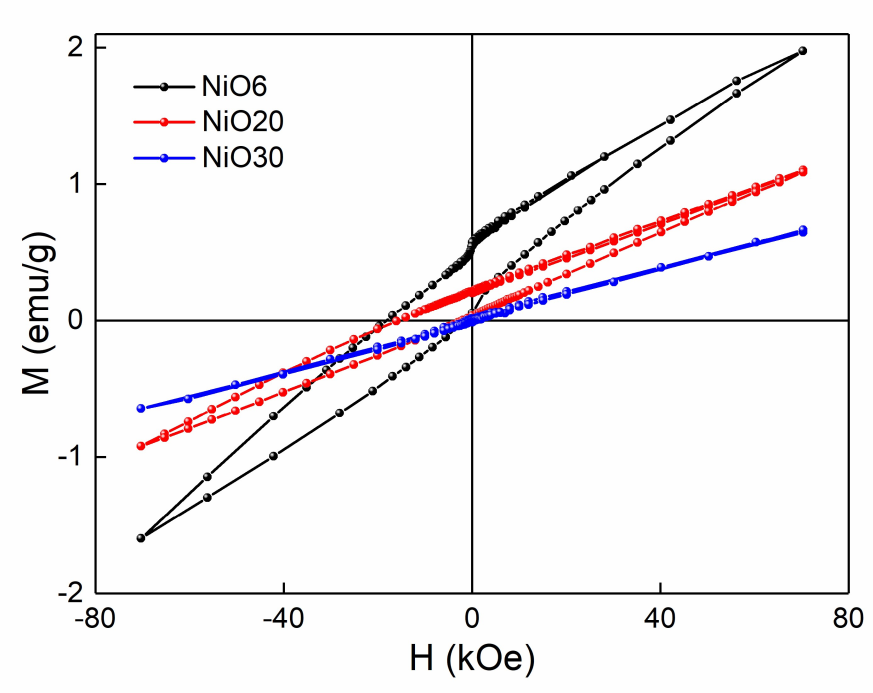

Figure S11. Hysteresis loops for samples NiO6 (black), NiO20 (red), NiO30 (blue) at 5 K after field cooling the samples under 5 kOe from room temperature. Field shifts increase significantly as the particle size decreases, from a negligible shift for sample NiO30 to 9.0(1) kOe for sample NiO6.

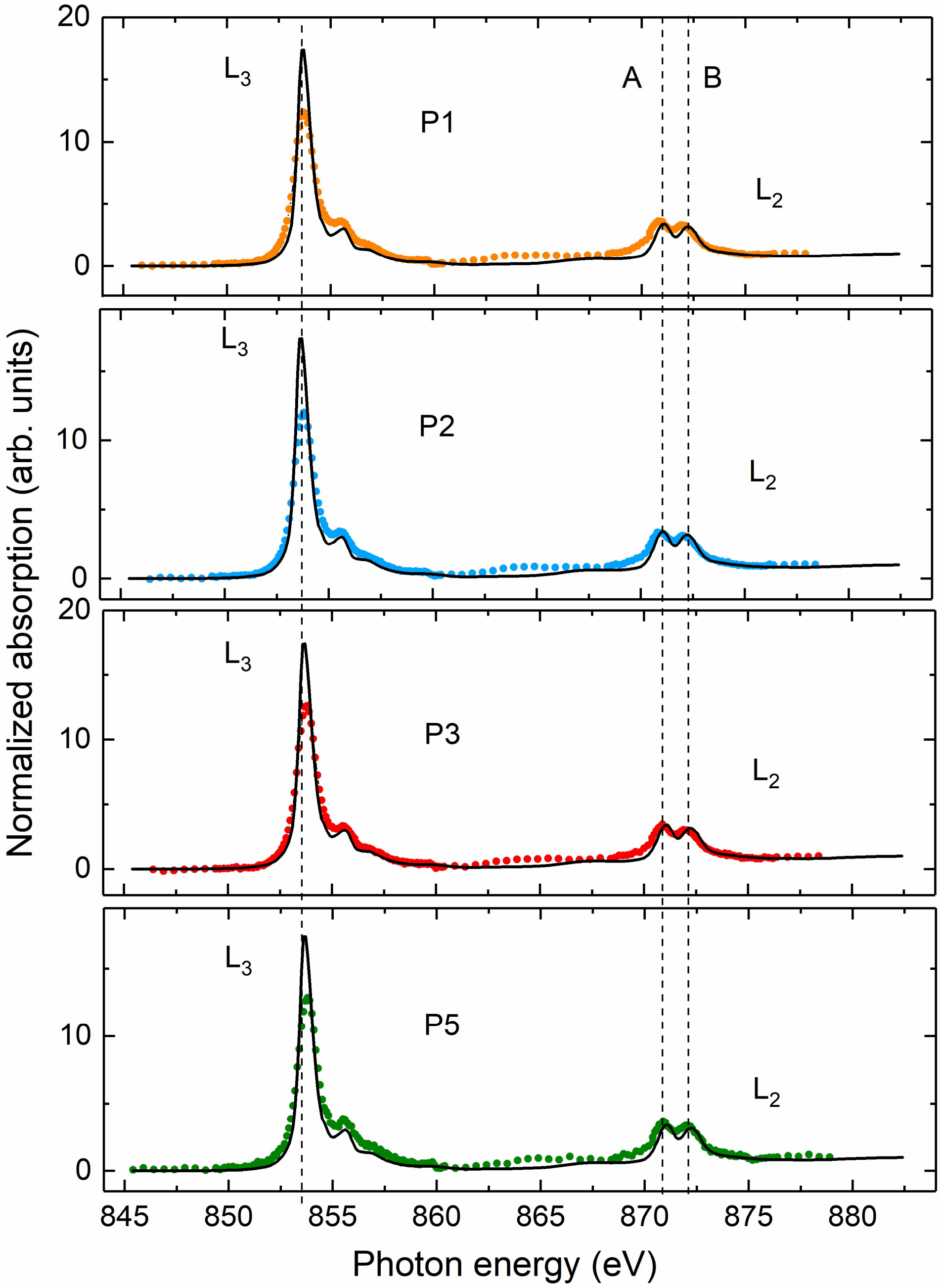

Figure S12. Gallery of isotropic, local Ni $L_{3,2}$-edge XAS spectra recorded for particles P1 (orange symbols), P2 (blue symbols), P3 (red symbols), and P5 (green symbols) in the XPEEM image in Fig. 6(b) compared with fits (black solid lines) to a weighted linear combination of the reference bulk spectra of both Ni and NiO taken from Refs. [1], [2] in the Supplementary information. All the individual particles for the XMLD-XPEEM study are compatible with a single NiO phase within an error bar of up to 7%.

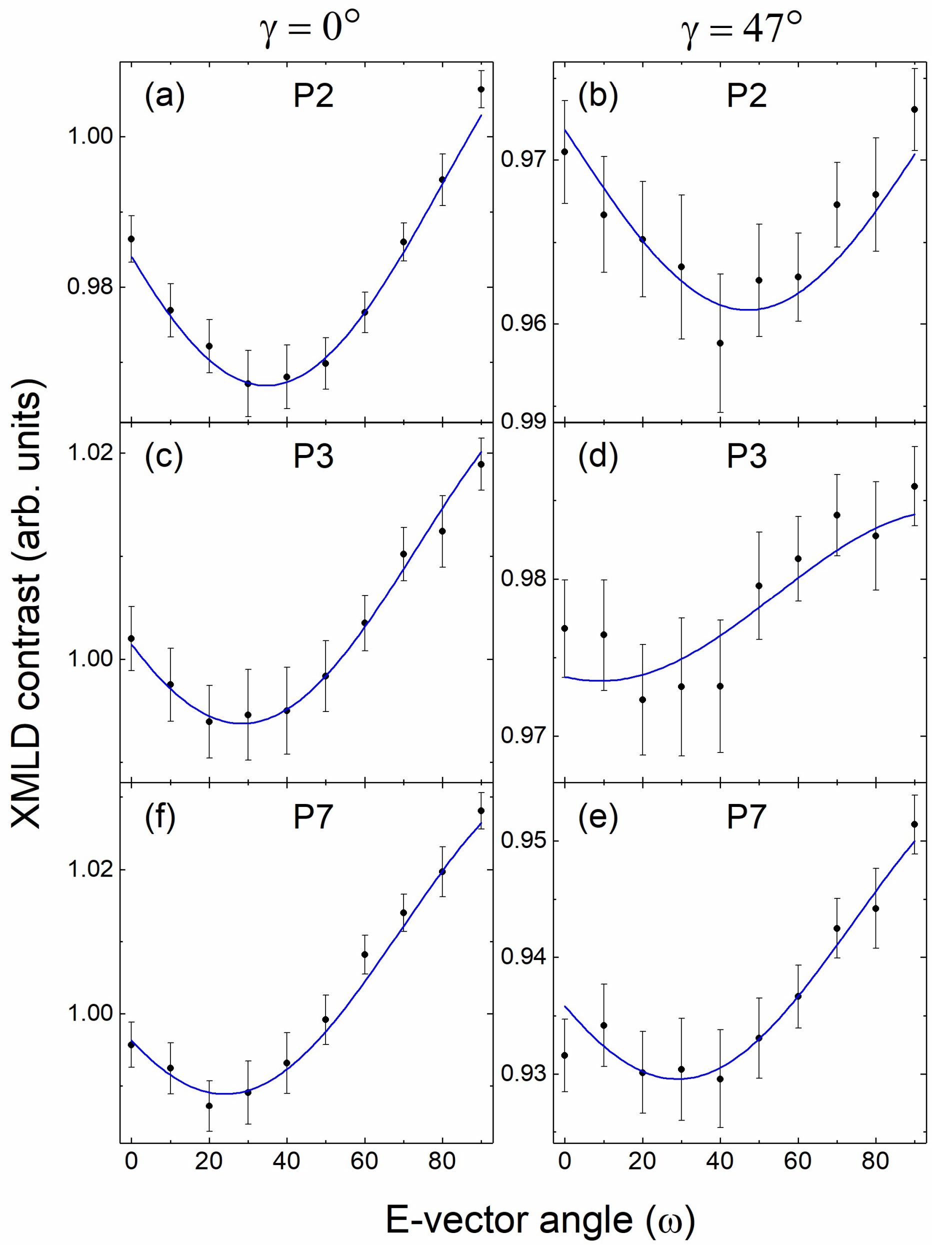

Figure S13. Experimental XMLD data (symbols) along with their corresponding fits to Eqs. 6 and 7 (blue solid lines) for three of the particles shown in Fig. 7 (P2, P3, and P7).

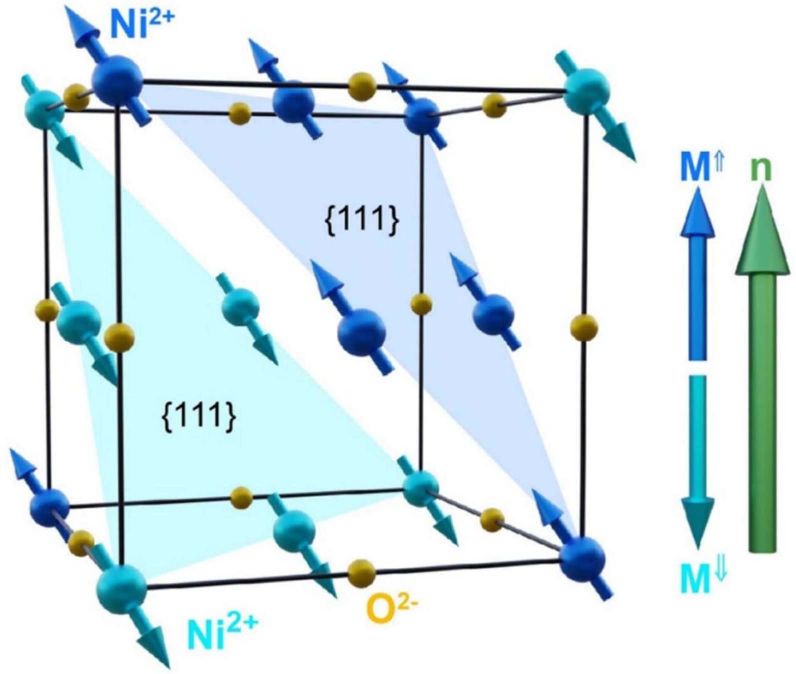

Figure S14. The crystallographic and magnetic structure of NiO is illustrated, highlighting the two Ni^{2+} sublattices (M↑ and M↓) in the {111} planes referred to the simple cubic lattice and defining the Néel vector as $\mathbf{n} \equiv M\uparrow - M\downarrow$ along the ⟨112⟩ directions, following Ref. [3] in the Supplementary information.

References

1. Regan, T. J. (2001). X-ray Absorption spectroscopy and microscopy study of ferro- and antiferromagnetic thin films, with applications to exchange anisotropy. PhD Thesis, Standford University.

2. Regan, T. J.; Ohldag, H.; Stamm, C.; Nolting, F.; Lüning, J.; Stöhr, J.; White, R. L. Chemical effects at metal/oxide interfaces studied by X-ray-absorption spectroscopy. *Phys. Rev. B* **2001**, *64*, 214422.

3. Gomonay, O.; Bossini, D. Spin dynamics in antiferromagnets. *J. Phys. D: Appl. Phys.* **2021**, *54*, 374004.